PHYSICAL REVIEW B **96**, 085408 (2017)

Excited-state indirect excitons in GaAs quantum dot molecules

Ch. Heyn, A. Küster, A. Ungeheuer, A. Gräfenstein, and W. Hansen
Institut für Nanostruktur- und Festkörperphysik (INF), Universität Hamburg, Jungiusstraße 11, D-20355 Hamburg, Germany
(Received 30 March 2017; revised manuscript received 12 June 2017; published 4 August 2017)

We demonstrate the fabrication of strain-free and widely adjustable GaAs quantum-dot molecules (QDMs) by filling of droplet etched nanoholes in AlGaAs. Gate-voltage dependent optical spectra of highly asymmetric QDMs exhibit anticrossings that clearly indicate strong coupling with delocalized molecule states. Furthermore, indirect excitons are observed that are related to recombinations of excited-state electrons and ground-state holes both located in different dots. Simple numerical simulations reproduce the electric-field dependent energy shifts of direct and indirect transitions and predict their radiative lifetimes. The visibility of excited-state indirect excitons even for strong off-resonant energy detuning indicates the presence of a phonon bottleneck which suppresses the relaxation of excited electrons into lower levels.

DOI: 10.1103/PhysRevB.96.085408

I. INTRODUCTION

Closely spaced semiconductor quantum dot (QD) pairs with significant interdot coupling are called a quantum-dot molecule (QDM) [1–4] in analogy to natural molecules like hydrogen. The coupling phenomena itself represent an interesting field of fundamental research [2,3]. Furthermore, this artificial coupled quantum system has potential applications, e.g., in quantum information processing [5] as a quantum gate [4,6,7]. The QDM optical emission shows prominent features like anticrossings indicating tunnel-coupled resonances with bonding and antibonding states or indirect excitons with electrons and holes residing in different dots [8,9]. The occurrence of these features also for excited states is controlled by the balance of the lifetimes for radiative recombination and relaxation. Excited-state anticrossings are observed [3] since the relaxation of delocalized excited-state charge carriers at resonance into lower states localized in one of the two dots has a small probability. On the other hand, off-resonant indirect excitons with excited-state charge carriers are not expected since here usual relaxation times of a few 100 ps [10,11] are much faster than the radiative lifetimes.

In this work, we report strongly asymmetric GaAs QDMs with excited-state indirect excitons visible even for a very strong off-resonant detuning. This surprising finding is explained by exited-state electrons being conserved by a suppression of relaxation due to a phonon bottleneck [10–12].

For the self-assembled QDM fabrication often strain-induced vertical ordering is utilized, e.g., Stranski-Krastanov QDMs composed of two InAs QDs [3,4,6,9]. However, such QDMs are substantially strained and the tunability of the individual dot sizes is limited. The present strain-free GaAs QDMs are fabricated in a different way by filling of nanoholes in AlGaAs surfaces. The nanoholes are created in a self-assembled fashion using local droplet etching (LDE) [13,14]. The whole process is fully compatible with conventional molecular beam epitaxy (MBE). GaAs QDs fabricated by LDE exhibit an optical emission adjustable from 700 to 800 nm [15], sharp exciton peaks [16], an exciton fine-structure splitting down to 5 μeV [17], and clear single-photon emission [17]. Most importantly here, the size and quantum level structure of the two dots forming the QDM can be chosen to be very different.

II. FABRICATION OF GaAs QDMS

A schematic of the QDM fabrication is shown in Fig. 1(a). The process is described in detail in Ref. [17]. In brief, a 50 nm thick Si-doped (1×10^{18} cm^{-3}) GaAs back gate and a 120 nm thick $Al_xGa_{1-x}As$ ($x = 0.33$) layer are grown on (001) GaAs substrates using solid-source MBE. For subsequent LDE, the As_4 flux is reduced by a factor of at least one hundred with respect to typical GaAs growth conditions and Al droplets are formed during deposition of 1.0 monolayers (ML) of Al at $T = 630\,^{\circ}$C. The droplets are transformed into about 28 nm deep nanoholes with density of about 1.5×10^7 cm^{-2} during 180 s postgrowth annealing at unchanged T [14]. For QDM fabrication, the nanoholes are filled by deposition of nominally $d_B = 0.45$ nm GaAs to form the bottom dot QD_B, followed by $d_{TB} = 3$–5 nm AlGaAs or AlAs for the tunnel barrier (TB), and $d_T = 0.55$–1.35 nm GaAs for the top dot QD_T. Finally, a 73 nm thick AlGaAs cap layer is grown. We note that the GaAs layers deposited for hole filling form quantum wells [Fig. 1(a)] similar to the wetting layer for Stranski-Krastanov QDs.

III. BASIC QDM OPTICAL PROPERTIES

Figure 1(b) shows a low temperature photoluminescence (PL) spectrum from a QDM with $d_T = 0.88$ nm, an AlAs TB of $d_{TB} = 3$ nm, and no top gate. For excitation either a cw laser at $\lambda = 532$ nm is used for nonresonant excitation into the AlGaAs barrier or a pulsed laser at $\lambda = 640$ nm for time-resolved measurements [18]. Clearly visible are the exciton peaks X from QD_B and QD_T, respectively. For samples with AlAs TB, the measured linewidths are 80–110 μeV for QD_B and 80–150 μeV for QD_T. Samples with AlGaAs TB show much broader peaks with linewidth of several 100 μeV [17]. The reason for this observation is not clear, so far. The QDM in Fig. 1(b) is highly asymmetric: the ground-state emission from the low energy QD_B and QD_T differs by 152 meV. Figure 1(c) demonstrates the independent tunability of the QD emission energies by the respective nanohole filling levels. An increase of d_T yields a redshifted emission from QD_T, whereas the PL energy of QD_B is nearly constant. Furthermore, samples with AlAs TB have higher QD_T emission energy due to the stronger confinement. Variation also of d_B allows the fabrication of QDMs with equal emission energies from both dots (not shown here).

 ©2017 American Physical Society

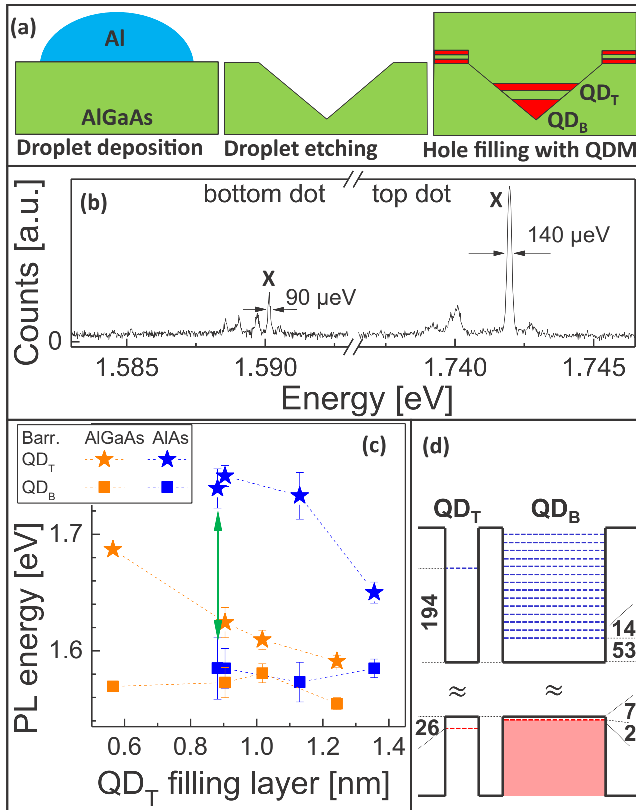

FIG. 1. (a) Schematic of the QDM fabrication process with droplet material deposition, self-assembled droplet etching, and hole filling with QD_B, tunnel barrier, and QD_T. (b) Micro-PL measurement at $T = 8$ K of a single QDM with $d_B = 0.45$ nm, $d_T = 0.88$ nm, and AlAs tunnel barrier of $d_{TB} = 3$ nm. The exciton peaks are marked by X and the respective linewidths are given. (c) QD_T and QD_B PL ground-state energies from samples with varied d_T and tunnel barrier material (AlGaAs or AlAs), $d_B = 0.45$ nm, and $d_{TB} = 3$–5 nm. The error bars represent measurements of 5 to 10 QDMs from each sample. Green arrows mark the sample that is discussed in this paper. (d) Schematic band diagram of the studied QDMs with average ground-state and quantization energies in meV. Note that the band gap does not scale with the size quantization as indicated by the ≈ signs.

The present work focuses on highly asymmetric QDMs with $d_B = 0.45$ nm, $d_T = 0.88$ nm, and $d_{TB} = 3$ nm [green arrows in Fig. 1(c)]. These QDMs show PL ground-state energies of 1.58 ± 0.03 eV for QD_B and 1.74 ± 0.02 eV for QD_T as well as quantization energies (first exited state minus ground state) of 16 ± 5 meV (QD_B) and 19 ± 3 meV (QD_T). The quantization energies are determined from PL spectra taken under higher excitation power where due to shell filling with multiexciton complexes the QD shell structure becomes visible [15]. Figure 1(d) shows a schematic band diagram of a QDM where the energies of the electron and hole states are estimated from the above PL data using the electron and hole effective masses and under assumption of a parabolic potential with equidistant energy levels. According to this, resonant electron levels are expected between QD_T ground state and roughly the tenth or eleventh state in QD_B.

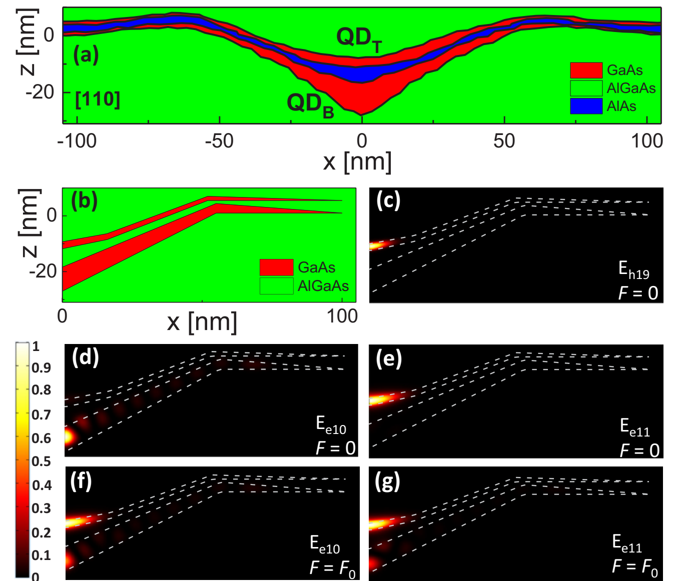

FIG. 2. (a) AFM line scans with equal x- and y-axis scales along [110] direction from a sample series illustrating the different interfaces during QDM fabrication, i.e., the initial nanohole in the AlGaAs substrate (green), the hole filled with QD_B (red), the AlAs tunnel barrier (blue), QD_T (red), and the AlGaAs cap layer (green). The baselines of the individual AFM scans are offset by the respective deposited layer thickness. (b) Approximated QDM shape used for the simulations. The QD axis is at $x = 0$ and the dot is rotational symmetric to this axis. (c) Simulated square of the wave function of the 19th QDM hole level representing the QD_T hole ground state at $F = 0$. (d) The 10th QDM electron level at $F = 0$, (e) the 11th QDM electron level representing the QD_T electron ground state at $F = 0$, (f) the 10th QDM electron level at $F = F_0 = 5$ kV/cm (resonance), and (g) the 11th QDM electron level at $F = F_0$.

IV. SIMULATION OF QDM OPTICAL EMISSION

We perform finite-element simulations for a more detailed interpretation of the QDM electronic levels. The single-particle simulation is based on an effective mass approximation in cylindrical symmetry and simulates the wave functions Ψ and the quantized energy levels [19]. For electrons, the first 20 energy levels are calculated and the first 30 levels for holes. The PL emission energy is simply approximated from the GaAs band-gap energy and the energy difference of the single-particle electron and hole levels neglecting Coulomb interaction effects. We have started with simple cone-shaped QDs and determined their height and diameter by comparison of simulated ground state and quantization energies with the above PL results. In the next step, the cones are folded for more realistic dot shapes based on atomic-force microscopy (AFM) data. Figure 2(a) shows AFM line scans from a sample series where the fabrication process has been stopped at the different interfaces. The hole depths vary by ±10% over a sample and typical holes with depth close to the average value were selected. Obviously, bottom and top dot have substantially different shapes due to the nanohole template. The smaller extend of QD_T in growth direction is the reason for its higher PL energy. Furthermore, the tunnel barrier has a nonuniform thickness with a maximum at the QDM axis.

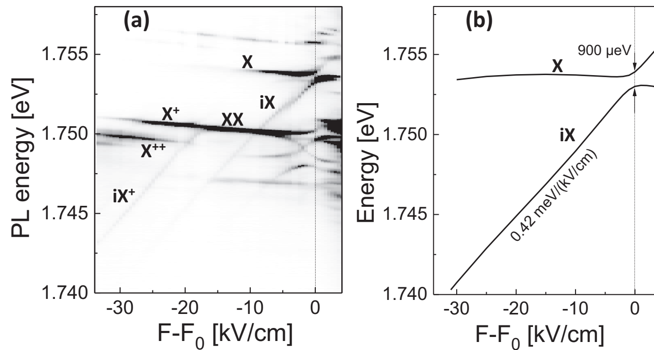

FIG. 3. (a) Gray-scale plot of the PL emission intensity at $T = 8$ K from the top dot of a GaAs QDM as function of electric field F varied by a gate voltage. (b) Simulated energy of a direct exciton X (E_{e11}, E_{h19}) and indirect exciton iX (E_{e10}, E_{h19}) at varied F. The electric field is given relative to the field F_0 at resonance.

Figure 2(b) shows the approximated QDM geometry used for the simulations. Simulated probability densities Ψ^2 of a QDM without external field are shown color encoded in Figs. 2(c)–2(e). For holes, the nineteenth QDM state E_{h19} [Fig. 2(c)] is the lowest state localized in QD_T. The electron QDM states 1–10 [Fig. 2(d)] are well localized in QD_B while the eleventh state E_{e11} [Fig. 2(e)] is predominantly found in QD_T. This identifies the ground-state PL emission from QD_T (direct exciton, X) as a transition between E_{e11} and E_{h19}.

V. FIELD DEPENDENCE OF QDM OPTICAL EMISSION

For field-dependent PL measurements the QDMs are embedded in a Schottky diode with an 18 nm thick evaporated Ti layer as optically transparent top gate. A gate voltage V_g is applied between top and back gate (distance 197 nm) to adjust a vertical electric field F. Figure 3(a) shows an example of the PL emission from a QDM top dot, where V_g is varied from 0.2 to 0.96 V. The electric field F is calculated from V_g relative to the field F_0 at resonance ($V_g = 0.88$ V). The strong PL lines with weak field dependence are related to direct excitons where electrons and holes reside in the top QD. The small extension of QD_T in field direction causes an only small Stark shift [20,21] of the direct exciton energy. The X and XX peaks are identified using additional excitation power dependent measurements [18], and the identification of the X^+ and X^{++} lines to positive singly and doubly charged exciton complexes bases on the assumption that at the corresponding fields the electrons more likely escape the quantum dots than the much heavier holes.

The PL data exhibit several features that are not visible in single-dot spectra. Striking and characteristic for quantum-dot molecule spectra are the indirect exciton and trion lines iX and iX^+ and the anticrossing of the indirect exciton iX with direct exciton X. The anticrossing of the trion lines iX^+ and X^+ is obscured by a strong biexciton line XX at almost the same energy. This biexciton line XX ramifies into a complex cross-shaped pattern with the center of the cross at $F - F_0 = -2$ kV/cm. Two branches of this pattern anticross at the same field $F = F_0$ where the direct and indirect exciton anticross. The anticrossing of the biexciton at the same field is readily explained by biexciton recombinations with the direct and indirect exciton as final states. Similar features have been observed, e.g., for InAs-QD based QDMs [3,9,22].

We focus here on the indirect exciton iX and its anticrossing with the direct exciton. The strong field dependence of the indirect exciton is caused by recombinations of electrons and holes located in different dots of the molecule [3,22,23]. The large distance between electron and hole involves a strong dipole moment and, thus, a large, mostly linear Stark shift of the line. The blueshift of the indirect exciton iX with increasing F indicates [9] that here a hole located in QD_T recombines with an electron in QD_B. The anticrossing between X and iX at $F = F_0$ [Fig. 3(a)] indicates a molecule resonant state [3,4,9], where the measured energy splitting of about 500 μeV at resonance is caused by the energy separation between bonding and antibonding states. Since the hole resides in QD_T for both X and iX, this anticrossing is related to tunnel coupling of an electron in the ground state of QD_T and an excited state of QD_B.

From a comparison with the simulations we estimate the energy levels of the iX transition. We have already identified the QD_T ground-state direct exciton X as a transition between the QDM states E_{e11} and E_{h19} [Figs. 2(e) and 2(c)]. At resonance ($F = F_0 = 5$ kV/cm), the simulated QD_B excited electron state E_{e10} couples with the QD_T ground-state electron level E_{e11}. Figures 2(f) and 2(g) show that the electron wave functions are spread among both dots for the two levels. Thus the indirect exciton iX represents a transition between the QDM states E_{e10} and E_{h19}. Figure 3(b) shows the simulated field dependence of the X and iX transition energy. The simulated slopes of X and iX agree quantitatively with the experimental data, whereas the splitting at resonance is approximately doubled in the simulations. This is a reasonable agreement in view of the fact that Coulomb attraction is not considered in the simulation.

VI. EXCITED-STATE INDIRECT EXCITONS

The observation of the excited-state indirect exciton iX over a vast field range represents a major result of this work. In the PL spectra, the iX peak is visible even for a strong off-resonant energy detuning up to 11 meV [Fig. 3(a)]. The optical emission from excited states is controlled by the lifetimes of the competing processes recombination and relaxation. Usually, QD levels are filled in ascending energetic order since relaxation of excited-state charge carriers into lower energy levels is faster than recombination. Holes with small level spacing relax via direct emission of acoustical phonons. For electrons with larger level spacing the situation is more complex. Direct electron relaxation by phonon emission under momentum conservation has a very low probability, which is known as the so-called phonon bottleneck [10–12]. On the other hand, short lifetimes of a few 100 ps [10] have been predicted for indirect relaxation via electron-hole scattering [10,11] in GaAs QDs. Here, electron-hole scattering means that an electron in an excited state transfers energy to a hole in the same dot and, thus, relaxes without direct phonon emission.

The lifetimes τ_X and τ_{iX} of X and iX radiative recombinations are estimated from the simulated overlap integral of

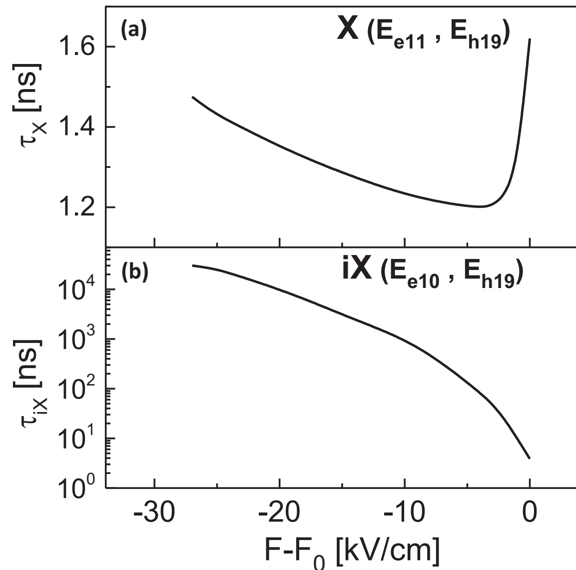

FIG. 4. (a) Lifetimes of X and (b) iX at varied F. The lifetimes are calculated from the overlap integral $\langle\Psi_e|\Psi_h\rangle^2$ of the simulated electron and hole wave functions according to Fermi's golden rule [24].

the electron and hole wave functions $\langle\Psi_e|\Psi_h\rangle^2$ using a model [24] that is based on Fermi's golden rule. Results are plotted in Figs. 4(a) and 4(b). The simulations yield an only weak field dependence of $\tau_X = 1.2$–1.6 ns of the direct exciton which is in reasonable agreement with values of 1.9 ± 0.8 ns we measure with time-resolved PL. On the other hand, simulated τ_{iX} for indirect transitions show a much stronger field dependence with maximal values longer than ten microseconds for $F - F_0 < -20$ kV/cm. The low intensity does not allow lifetime measurements of iX transitions with our setup. As a key point, the calculated τ_{iX} is orders of magnitude longer than the lifetime for fast relaxation by electron-hole scattering. Thus the experimentally observed off-resonant iX emission clearly indicates that significant electron-hole scattering can be excluded. Since our PL measurements typically integrate over 10 s and, thus, include a large number of recombination processes, as an obvious explanation we assume that there are periods of time longer than τ_{iX} during which the hole population in QD_B is zero and that electron-hole scattering events are suppressed by a phonon bottleneck [10,11].

Furthermore, the PL spectrum in Fig. 1(b) demonstrates an only weak exciton peak intensity from the larger QD_B compared to the smaller QD_T. This is in contrast to the usually in tunnel-coupled asymmetric QDMs observed trend where at low excitation power the emission from the larger low-energy dot dominates [25]. The inverse PL signature of the present QDMs agrees with the above assumption of a partly zero hole population in QD_B.

The following scenario is suggested to explain the above results. Excitons are generated by laser irradiation dominantly in the barrier material surrounding the QDMs. The excitons can diffuse into the QDs and recombine there. This causes the direct exciton recombination peak X in QD_T. On the other hand, the phonon bottleneck for relaxation of excited-state electrons in QD_B indicates there a partly zero hole population and, thus, an only small exciton diffusion into the bottom dot. We assume that this asymmetric exciton diffusion might be related to the GaAs quantum wells deposited for QDM generation which guide the excitons mainly into QD_T. The excited-state electrons are injected into QD_B by tunneling from QD_T and stabilized with lifetimes of tens of microseconds by a phonon bottleneck since the distant hole in the top dot does not allow fast relaxation via electron-hole scattering. Tunneling of holes is suppressed due to their higher effective mass. The long lifetime of bottom dot excited-state electrons enables indirect transitions with holes in QD_T despite the small wave function overlap.

In Refs. [22,23] a detuning of a few meV was reported for ground-state indirect excitons where relaxation is not possible. Reference [3] shows in addition data from excited-state indirect excitons with a maximum detuning of only a few 100 μeV. We assume that there a fast relaxation by electron-hole scattering suppresses off-resonant indirect transitions.

VII. CONCLUSIONS

In conclusion, a self-assembled fabrication scheme for coupled GaAs quantum dot molecules is demonstrated which allows the creation of highly asymmetric QDMs. Their unique properties enable the coupling between the ground state in one dot and a highly excited state in the second dot thus forming a metastable, highly excited quantum mechanical system. With the large energy and field range, in which coupling is observed in the asymmetric QDMs, intriguing studies of phonon and Auger-type relaxation mechanism as well as conditional quantum dynamics [6] become possible. Moreover, the wide tunability of the indirect exciton radiative lifetime can be used for the realization of a voltage-adjustable delay line for single photons.

ACKNOWLEDGMENTS

The authors would like to thank the "Deutsche Forschungsgemeinschaft (DFG)" for financial support via GrK 1286, HA 2042/6-1, and HA 2042/8-1.

[1] *Quantum Dot Molecules*, edited by J. Wu and Z. M. Wang, Series: Lecture Notes in Nanoscale Science and Technology Vol. 14 (Springer, New York, 2014).

[2] M. Bayer, P. Hawrylak, K. Hinzer, S. Fafard, M. Korkusinski, Z. R. Wasilewski, O. Stern, and A. Forchel, Science **291**, 451 (2001).

[3] M. Scheibner, M. Yakes, A. S. Bracker, I. V. Ponomarev, M. F. Doty, C. S. Hellberg, L. J. Whitman, T. L. Reinecke, and D. Gammon, Nat. Phys. **4**, 291 (2008).

[4] K. Müller, A. Bechtold, C. Ruppert, M. Zecherle, G. Reithmaier, M. Bichler, H. J. Krenner, G. Abstreiter, A. W. Holleitner, J. M. Villas-Boas, M. Betz, and J. J. Finley, Phys. Rev. Lett. **108**, 197402 (2012).

[5] D. DiVincenzo, Science **270**, 255 (1995).
[6] L. Robledo, J. Elzerman, G. Jundt, M. Atatüre, A. Högele, S. Fält, and A. Imamoglu, Science **320**, 772 (2008).
[7] D. Kim, S. G. Carter, A. Greilich, A. S. Bracker, and D. Gammon, Nat. Phys. **7**, 223 (2011).
[8] H. J. Krenner, M. Sabathil, E. C. Clark, A. Kress, D. Schuh, M. Bichler, G. Abstreiter, and J. J. Finley, Phys. Rev. Lett. **94**, 057402 (2005).
[9] A. S. Bracker, M. Scheibner, M. F. Doty, E. A. Stinaff, I. V. Ponomarev, J. C. Kim, L. J. Whitman, T. L. Reinecke, and D. Gammon, Appl. Phys. Lett. **89**, 233110 (2006).
[10] I. Vurgaftman and J. Singh, Appl. Phys. Lett. **64**, 232 (1994).
[11] J. Urayama, T. B. Norris, J. Singh, and P. Bhattacharya, Phys. Rev. Lett. **86**, 4930 (2001).
[12] U. Bockelmann and G. Bastard, Phys. Rev. B **42**, 8947 (1990).
[13] Z. M. Wang, B. L. Liang, K. A. Sablon, and G. J. Salamo, Appl. Phys. Lett. **90**, 113120 (2007).
[14] Ch. Heyn, Th. Bartsch, S. Sanguinetti, D. Jesson, and W. Hansen, Nanoscale Res. Lett. **10**, 67 (2015).
[15] Ch. Heyn, A. Stemmann, T. Köppen, C. Strelow, T. Kipp, M. Grave, S. Mendach, and W. Hansen, Appl. Phys. Lett. **94**, 183113 (2009).
[16] Ch. Heyn, A. Stemmann, T. Köppen, Ch. Strelow, T. Kipp, M. Grave, S. Mendach, and W. Hansen, Nanoscale Res. Lett. **5**, 576 (2010).
[17] A. Küster, C. Heyn, A. Ungeheuer, G. Juska, S. Tommaso Moroni, E. Pelucchi, and W. Hansen, Nanoscale Res. Lett. **11**, 282 (2016).
[18] Ch. Heyn, C. Strelow, and W. Hansen, New J. Phys. **14**, 053004 (2012).
[19] R. V. N. Melnik and M. Willatzen, Nanotechnology **15**, 1 (2004).
[20] S. A. Empedocles and M. G. Bawendi, Science **278**, 2114 (1997).
[21] J. J. Finley, M. Sabathil, P. Vogl, G. Abstreiter, R. Oulton, A. I. Tartakovskii, D. J. Mowbray, M. S. Skolnick, S. L. Liew, A. G. Cullis, and M. Hopkinson, Phys. Rev. B **70**, 201308(R) (2004).
[22] M. Scheibner, I. V. Ponomarev, E. A. Stinaff, M. F. Doty, A. S. Bracker, C. S. Hellberg, T. L. Reinecke, and D. Gammon, Phys. Rev. Lett. **99**, 197402 (2007).
[23] L. Wang, A. Rastelli, S. Kiravittaya, M. Benyoucef, and O. G. Schmidt, Adv. Mater. **21**, 2601 (2009).
[24] P. A. Dalgarno, J. M. Smith, J. McFarlane, B. D. Gerardot, K. Karrai, A. Badolato, P. M. Petroff, and R. J. Warburton, Phys. Rev. B **77**, 245311 (2008).
[25] Yu. I. Mazur, Zh. M. Wang, G. G. Tarasov, G. J. Salamo, J. W. Tomm, V. Talalaev, and H. Kissel, Phys. Rev. B **71**, 235313 (2005).